

Near UV-Irradiation of CuOx-Impregnated TiO2 Providing Active Species for H2 Production Through Methanol Photoreforming

Original

Near UV-Irradiation of CuOx-Impregnated TiO2 Providing Active Species for H2 Production Through Methanol Photoreforming / Vitiello, G.; Clarizia, L.; Abdelraheem, W.; Esposito, S.; Bonelli, B.; Ditaranto, N.; Vergara, A.; Nadagouda, M.; Dionysiou, D. D.; Andreozzi, R.; Luciani, G.; Marotta, R.. - In: CHEMCATCHER. - ISSN 1867-3880. - 11:17(2019), pp. 4314-4326. [10.1002/cctc.201900818]

Availability:

This version is available at: 11583/2767512 since: 2019-11-15T14:46:45Z

Publisher:

Wiley Blackwell

Published

DOI:10.1002/cctc.201900818

Terms of use:

openAccess

This article is made available under terms and conditions as specified in the corresponding bibliographic description in the repository

Publisher copyright

(Article begins on next page)

Heterogeneous & Homogeneous & Bio- & Nano-

CHEM **CAT** CHEM

CATALYSIS

Accepted Article

Title: Near UV-irradiation of CuOx-impregnated TiO₂ providing active species for H₂ production through methanol photoreforming

Authors: Giuseppina Luciani, Giuseppe Vitiello, Laura Clarizia, Wael Abdelraheem, Serena Esposito, Barbara Bonelli, Nicoletta Ditaranto, Alessandro Vergara, Mallikarjuna Nadagouda, Dionysios D. Dionysiou, Roberto Andreozzi, and Raffaele Marotta

This manuscript has been accepted after peer review and appears as an Accepted Article online prior to editing, proofing, and formal publication of the final Version of Record (VoR). This work is currently citable by using the Digital Object Identifier (DOI) given below. The VoR will be published online in Early View as soon as possible and may be different to this Accepted Article as a result of editing. Readers should obtain the VoR from the journal website shown below when it is published to ensure accuracy of information. The authors are responsible for the content of this Accepted Article.

To be cited as: *ChemCatChem* 10.1002/cctc.201900818

Link to VoR: <http://dx.doi.org/10.1002/cctc.201900818>

Accepted Article

Near UV-irradiation of CuO_x-impregnated TiO₂ providing active species for H₂ production through methanol photoreforming

Giuseppe Vitiello^[a,b], Laura Clarizia^{*,[a]}, Wael Abdelraheem^[c,d], Serena Esposito^[e],
Barbara Bonelli^[f], Nicoletta Ditaranto^[g], Alessandro Vergara^[h], Mallikarjuna Nadagouda^[i],
Dionysios D. Dionysiou^[c], Roberto Andreozzi^[a], Giuseppina Luciani^{*,[a]}, Raffaele Marotta^[a]

[a] Department of Chemical, Materials and Production Engineering (DICMaPI), University of Naples Federico II, p.le Tecchio 80, 80125 Naples, Italy.

[b] CSGI - Center for Colloids and Surface Science, via della Lastruccia 3, 50019 Sesto Fiorentino (FI), Italy.

[c] Environmental Engineering and Science Program, Department of Chemical and Environmental Engineering, 705 Engineering Research Center, University of Cincinnati, Cincinnati, OH 45221-0012, United States.

[d] Department of Chemistry, Faculty of Science, Sohag University, 82524 Sohag, Egypt.

[e] Department of Civil and Mechanical Engineering, University of Cassino and South of Lazio, Via G. Di Biasio 43, 03043 Cassino (FR), Italy.

[f] Department of Applied Science and Technology and INSTM Unit of Turin-Polytechnic, Polytechnic of Turin, C.so Duca degli Abruzzi 24, I-10129 Turin, Italy.

[g] Department of Chemistry, University of Bari Aldo Moro, via Orabona 4, 70125 Bari, Italy.

[h] Department of Chemical Sciences, University of Naples Federico II, Complesso di Monte S. Angelo, 80126 Naples, Italy.

[i] Department of Mechanical and Materials Engineering, Wright State University, Dayton, Ohio 45324, United States.

**Corresponding Authors:* Giuseppina Luciani (giuseppina.luciani@unina.it), Laura Clarizia (laura.clarizia2@unina.it)

Abstract

Copper doped-TiO₂ (P25) nanomaterials have been intensively studied as promising catalysts for H₂ production by photo-reforming of selected organic compounds. However, the role of copper oxidation states on the improvement of photocatalytic activity is still debated. In this work, CuO_x-impregnated P25-TiO₂ catalysts were used for photocatalytic production of hydrogen from methanol. Copper species/oxidation states both in the as-prepared catalysts and after the photocatalytic process were investigated. To this purpose, H₂ production rates were correlated to physico-chemical properties of the samples, both before and after photocatalytic process, by means of Raman, X-Ray Diffraction, Electron Paramagnetic Resonance spectroscopy, X-Ray Photoelectron Spectroscopy, Temperature-Programmed Reduction and High Resolution Transmission Electron Microscope techniques. Results revealed the presence of both Cu₂O and CuO deposits on the samples surface after calcination. Notably, under near-UV irradiation, the fraction of highly dispersed CuO particles undergo a partial dissolution process, followed by reduction to metallic copper Cu_(s) by photogenerated electrons, boosting H₂ production rate. Our findings indicate that both Cu₂O and Cu_(s) act as co-catalysts for H₂ generation, yet by different mechanisms. Overall this study, lies the basis to enhance catalytic performance of red-ox active systems through UV-irradiation approach.

Keywords: copper-based TiO₂, hydrogen production, photoreforming, photocatalysis, methanol.

Introduction

Limited availability of fossil fuels as well as their environmental impact has prompted scientific research towards cleaner and renewable energy sources. In this scenario, sunlight-driven H_2 production by either photo-reforming or water photo-splitting holds a great promise.^[1,2] However, photoreforming-based technologies have been far from practical application and suffer from poor efficiencies.^[1] Thus, improvement and optimization of photocatalytic systems are crucial tasks to make this technology feasible.^[3] Indeed, photocatalysts with appropriate band-gap and adequate stability for either organic photo-reforming or water-splitting under visible light irradiation with suitable energy efficiencies are still unavailable, and their development is considered a significant challenge in photocatalysis research.^[4,5]

Even though titanium dioxide in P25 form (80:20 w/w anatase:rutile) is considered one of the most promising commercial material for photocatalytic processes, it shows significant limitations, such as fast electron/hole recombination and absorption/activity restricted to the UV region due to its wide bandgap.^[6,7] Among the various methods employed for improving TiO_2 properties, doping with noble metals (Au, Pt, Pd) acting as co-catalysts has proven to be effective to enhance the photo-efficiency of titanium dioxide.^[3,8-10]

Alternatively, doping with transition metal ions such as Cu, Fe, Co, Ni is a cheaper promising option.^[6,9,11-13] The advantages of adopting these species lie in their behavior as electron scavengers, thus limiting charge recombination.^[9, 10, 14-16] In particular, copper loaded-P25 nanomaterials, prepared by impregnation method, have been proposed as promising catalysts for photo-reforming.^[17-19] Although several studies have investigated the effect of copper loading on P25 nanoparticles for the photocatalytic hydrogen generation through reforming of organics (Table 1), the effect of copper oxidation state on the improvement in photocatalytic activity, is not yet entirely clarified. Different conflicting opinions have been provided on synergistic effects of active copper species in photocatalytic reactions.

79 **Table 1** - Selected research papers devoted to testing Cu/P25 photocatalysts, prepared by
 80 impregnation method, in various photocatalytic processes.

Precursor	Calcination temperature (°C)	Cu oxidation state	Diagnostic technique	Application	Ref.
$\text{Cu}(\text{NO}_3)_2 \times 3\text{H}_2\text{O}$	300 – 500 for 0.5 h	CuO	TPR, XRD	Hydrogen production	[20]
$\text{Cu}(\text{NO}_3)_2 \times 2.5\text{H}_2\text{O}$	300 for 5 h (in air)	CuO	TPR	CO oxidation	[21]
$\text{Cu}(\text{NO}_3)_2 \times 2.5\text{H}_2\text{O}$	300 for 5 h (in air)	CuO/Cu ₂ O	TPR, XRD, XPS, Raman	CO oxidation	[22]
$\text{Cu}(\text{NO}_3)_2$	400 for 16 h (in air)	CuO	TPR, XRD, FTIR	Hydrogenation of 1,3-cyclooctadiene	[23]
$\text{Cu}(\text{CH}_3\text{COO})_2 \times \text{H}_2\text{O}$	250 for 4 h (in air)	Cu ²⁺ /Cu ⁺	TPR, XPS, FTIR	Hydrogenation of crotonaldehyde	[24]
$\text{Cu}(\text{NO}_3)_2$	400 for 1h (in Helium)	CuO/Cu ₂ O	TPR, XPS, FTIR,	CO oxidation	[25]
$\text{Cu}(\text{NO}_3)_2$	300 – 500 for 5 h	CuO/Cu ₂ O	DRS, XPS, FTIR	Hydrogen production	[26]
$\text{Cu}(\text{NO}_3)_2 \times 3\text{H}_2\text{O}$	300 for 0.5 h (in air)	CuO/Cu ₂ O	XPS, XRD	Hydrogen production	[27]
$\text{Cu}(\text{CH}_3\text{COO})_2 \times \text{H}_2\text{O}$ or $\text{Cu}(\text{NO}_3)_2$	500 – 600 for 1 h (in Argon)	CuO/Cu ₂ O	XRF, XRD	Acetic acid decomposition, hydrogen production	[28]
$\text{Cu}(\text{NO}_3)_2 \times 3\text{H}_2\text{O}$	400 for 2 h	CuO	XANES, EXAFS	Methylene blue degradation	[29]
$\text{Cu}(\text{NO}_3)_2$	350 for 4 h (in air)	CuO	XRD	Hydrogen production	[30]
$\text{Cu}(\text{NO}_3)_2 \times 3\text{H}_2\text{O}$	350 for 2 h (in air)	Cu ₂ O	XPS, XRD	Hydrogen production	[31]

$\text{Cu}(\text{NO}_3)_2$	100 – 600 n.r.	CuO	XPS, XRD	Hydrogen production	[32]
$\text{Cu}(\text{NO}_3)_2$	350 for 4 h (in air)	CuO	XRD	Hydrogen production	[33]
$\text{Cu}(\text{NO}_3)_2 \times 3\text{H}_2\text{O}$	450 for 4 h (in air)	CuO	XPS, XRD	Hydrogen production	[34]
$\text{Cu}(\text{NO}_3)_2 \times 3\text{H}_2\text{O}$	450 for 4 h (in air)	CuO , $\text{Cu}_x\text{Ti}_{1-x}\text{O}_2$	XRD, XANES, EXAFS	Hydrogen production	[35]
CuCO_2CH_3	400 for 1h (in air)	Cu_2O , CuO	XPS, XRD, DRUV	Gallic Acid degradation	[36]

81

82 Several studies report that Cu_2O species are responsible for enhanced photocatalytic H_2 production
83 from water.^[8,9,25,37] On the other hand, the presence of CuO was argued by different authors to be
84 responsible for the enhanced separation of photoinduced electrons and holes.^[3,30,32,33] Similarly,
85 Valero et al. proposed that easily reduced Cu^{2+} species could be responsible for higher Cu/P25
86 photoactivity.^[38] Other scientific studies also ascribe the improved photocatalytic activity of Cu/P25
87 systems to the presence of finely dispersed and easily reducible CuO_x (Cu^+/Cu) species on the TiO_2
88 surface.^[39] Such widespread variability in scientific conclusions is due to an intrinsic complexity of
89 materials during photocatalytic experiments, along with different impregnation procedures for copper
90 doping of P25 resulting in mixed oxidation states of copper on the catalyst surface. Typically, copper
91 exists in different oxidation states ($\text{Cu}_{(s)}$, Cu^+ , Cu^{2+}), that can change under UV-irradiation.^[40-42]
92 In this scenario, the present paper aims at elucidating the nature of copper species in Cu/ TiO_2
93 photocatalysts prepared via impregnation-calcination method. Moreover, evolution of copper species
94 under UV-irradiation during phot-reforming process was investigated, in order to clearly identify the
95 active species involved in H_2 production. Hydrogen production rates were compared and integrated
96 with a detailed physico-chemical characterization of the catalyst before and after the photo-catalytic

process, through a combined approach of complementary techniques, including X-Ray diffraction (XRD), X-Ray Photoelectron Spectroscopy (XPS), Raman and Electron Paramagnetic Resonance (EPR) Spectroscopies, Scanning Electron Microscopy (SEM), High Resolution Transmission Electron Microscopy (HR-TEM), and Temperature Programmed Reduction (TPR) analysis. This study is expected to deliver significant insights on the molecular factors responsible for the improved photocatalytic activity of Cu-based TiO₂ materials, thus providing critical guidelines for the design of new copper doped photocatalysts for UV-solar photoreforming.

Results and Discussion

Photocatalytic tests

Effect of photocatalyst copper content on H₂ generation

P25-based samples with different copper weight percentages, in the range 0.5-16 wt%, were tested for hydrogen generation through photoreforming of methanol. Figure 1A shows H₂ production rate of Cu(3%)/P25 after calcination at 350 °C; this trend, approaching a plateau within about 120 minutes, is representative of all compositions. During the photocatalytic run, the suspension turned from light teal to deep indigo, thus suggesting that a change in copper oxidation state occurred under UVA irradiation.^[27] After 180 minutes of reaction, UVA radiation was cut off by inserting a NaNO₂ solution (1 M) into the cooling system, as previously proposed and described in the Experimental section.^[43] Such procedure allowed to test the photocatalytic activity under only visible light irradiation. No hydrogen generation was recorded for any catalysts tested under only visible light irradiation, thus indicating that such system are activated by UV irradiation. Furthermore, hydrogen production rates were remarkably higher than values obtained over bare P25-TiO₂ calcined under inert atmosphere at 350 °C for 5 hours (0.55 μmol/min) and comparable to the values measured by Jung et al. by using H₂-treated Cu/P25 samples.^[27] Figure 1B depicts the change in solution pH during the photoreforming run. There was no changes in pH, which kept constant at about 6.5 throughout the experiment. Furthermore, no trace of dissolved copper was detected throughout the experiment, thus suggesting

a high stability of the photocatalyst. Figure 1C shows hydrogen production rate as a function of copper content. A non-monotonic trend was observed, with catalysts containing 3% and 6% weight percentages of copper displaying comparable similar values of hydrogen production rate, which were also the highest recorded. All Cu/P25 systems showed higher light absorption capability than bare P25-TiO₂ both in the UV and visible range (Figure S1A-B), although this did not result in a catalytic activity of the Cu-doped catalyst under visible light irradiation.

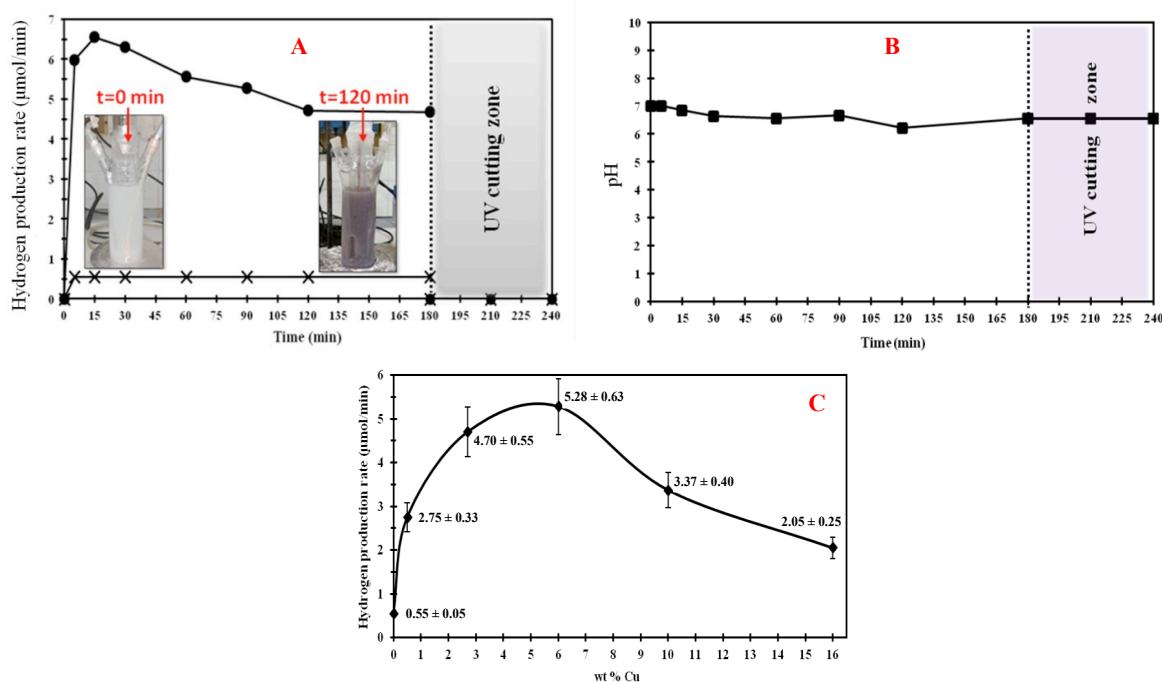


Figure 1. Panel A: Hydrogen production rate over (●) Cu(3%)/P25 and (×) bare P25-TiO₂, both calcined under inert atmosphere at 350 °C for 5 hours. After 180 minutes of reaction, UVA radiation has been cut off by inserting 1 M NaNO₂ solution into the cooling system. Catalysts load =150 mg/L. [CH₃OH]₀ = 2.47 M. T=25 °C. P=1 atm. The insets represent the colour suspension with Cu(3%)/P25 before and after 120 min of reaction. **Panel B:** Solution pH throughout the photoreforming run over Cu(3%)/P25 catalyst calcined under inert atmosphere at 350 °C for 5 hours. After 180 minutes of reaction, UVA radiation was cut off by inserting 1M NaNO₂ solution into the cooling system. Cu(3%)/P25 catalyst load=150 mg/L. [CH₃OH]₀ = 2.47 M. T=25 °C. P=1 atm). For each value, 12% error was considered, based on the results of a reproducibility photoreforming run performed over Cu(3%)/P25 calcined at 350 °C. **Panel C:** Plateau values of hydrogen production rate recorded over P25-TiO₂ catalysts calcined under inert atmosphere at 350 °C for 5 hours with different copper content. Weight percentages of copper: 0.5%, 3%, 6%, 10%, 16%. Cu/P25-TiO₂ catalysts load=150 mg/L. [CH₃OH]₀ = 2.47 M. T=25 °C. P=1 atm.

Effect of photocatalyst calcination temperature on H₂ generation

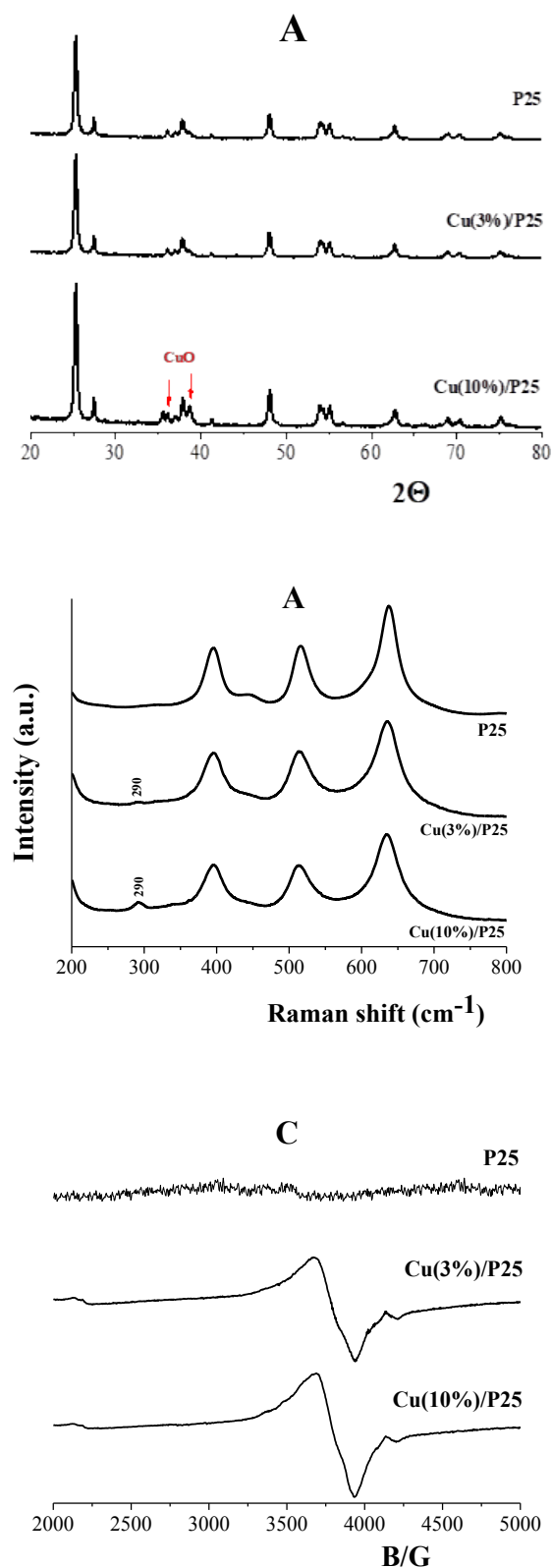
Cu/P25 samples calcined under inert N₂ atmosphere for 5 hours at different temperatures were tested for hydrogen generation through photo-reforming of methanol. Calcination temperatures were

investigated in the range of 150-550 °C (Figure S2, Supplementary Information). Similar values of hydrogen generation rates were achieved by using catalysts calcined at 150-350 °C, though, further increase in calcination temperature showed detrimental results in terms of photoefficiency for hydrogen generation. Once again, no hydrogen evolution was recorded by excluding UV irradiation for all catalysts tested.

Characterization of the fresh photocatalysts

Detailed physico-chemical characterizations of Cu/P25 samples were carried, before and after photocatalytic experiments, in order to investigate changes in catalysts' properties upon use for H₂ production under near-UV irradiation. In particular, copper oxidation states in Cu deposited species on P25 surface were assessed both before and after photocatalytic experiment with the aim of revealing their role in the enhancement of photocatalytic H₂ production. The measured values of BET surface specific area (S_{BET}) for Cu/P25 catalysts calcined at different temperatures or with different Cu loads are summarised in Table S1 (Supplementary Information). No particular changes were observed before and after use (data not shown), but a significant decrease in the surface area was recorded for the catalyst calcined at 550 °C, likely due to some aggregation phenomenon. Specifically, the highest surface area of 41 m²/g was recorded for Cu(3%)/P25 calcined at 350 °C. XRD spectra were collected in order to assess crystalline properties in the catalysts. Figure 2A shows XRD spectra of bare P25, fresh Cu(3%)/P25 and Cu(10%)/P25 calcined at 350 °C for 5h. Peaks of anatase and rutile structures appeared in all samples. Furthermore, XRD profiles of the fresh Cu(3%)/P25 samples did not show any diffraction peaks of CuO_x species, in agreement with the low amount of Cu. On the contrary, XRD spectrum of Cu(10%)/P25 sample highlighted two diffraction peaks at about 36.5° and 38.5°, displaying the presence of CuO.^[27] Comparison of the peak intensities of rutile and anatase revealed the typical composition of P25 samples that was not altered neither by Cu impregnation (Figure 2A). Furthermore, no relevant changes in peak position and intensity were

172 appreciated the XRD patterns of samples treated up to 450 °C (Figure S3), revealing that thermal
173 treatment did not significantly alter the samples crystalline structure.



174

175 **Figure 2.** XRD patterns (**panel A**), Raman spectra (**panel B**) and normalized EPR spectra (**panel C**)
176 of bare P25, fresh Cu(3%)/P25 and Cu(10%)/P25 calcined at 350 °C for 5h.

177 Raman and EPR spectra were also recorded in order to define the oxidation state of copper
178 impregnated on the P25 surface for materials before their use (Figure 2B-C). Concerning the fresh
179 Cu/P25 catalyst, Raman spectra were recorded on Cu(3%)/P25 and Cu(10%)/P25 samples (Figure
180 2B) also compared to P25 as reference material. Both catalysts showed a peak at 290 cm^{-1} , which is
181 ascribable to the Raman band of CuO. Although it is usually detected around 279 cm^{-1} , and is
182 associated to an A_g mode,^[45] the upshift in wavenumbers observed in our experiments compared to
183 pure CuO can occur either due different structuring or to interactions with the hosting matrix (herein
184 TiO_2). On the other hand, the typical most intense Raman band of Cu_2O and corresponding to the
185 second order overtone $2\Gamma_{12^-}$ (216 cm^{-1})^[44] was never visible in any analysed catalyst (Figure 2B). The
186 presence of cupric species in pre-used (fresh) Cu(3%)/P25 and Cu(10%)/P25 catalysts was also
187 confirmed by EPR spectra (Figure 2C) showing an asymmetric signal for both samples at a g-factor
188 of ~ 2.0800 , which is larger than the g-value of free electron $g_e = 2.0023$ and is related to the presence
189 of Cu^{2+} in the distorted octahedral coordination of TiO_2 .^[46] The broadness of the EPR spectra indicates
190 the presence of dipolar interaction among neighboring Cu^{2+} ions that leads to the increase in the width
191 of the EPR signal.

192 Therefore, XRD, EPR and Raman analyses confirm the presence of CuO in Cu/P25 samples.
193 Morphology, crystal structure and copper oxidation states were also assessed through TEM analyses.
194 Figure 3A shows HR-TEM and Fast Fourier Transform (FFT) analyses for fresh Cu(3%)/P25 sample
195 calcined at 350°C . An interplane distance of $d_{\text{Cu}} = 0.231\text{ nm}$ calculated from the HR-TEM micrograph
196 (Figure 3A), corresponding to the (111) plane of CuO, further confirmed its presence on TiO_2 (d_{TiO_2}
197 $= 0.33\text{ nm}$), in accordance with XRD, Raman and EPR results. Moreover, FFT image (*inset* of Figure
198 3C) clearly justified the existence of TiO_2 material in amorphous structure with some clear spots
199 related to the co-existed CuO particles.

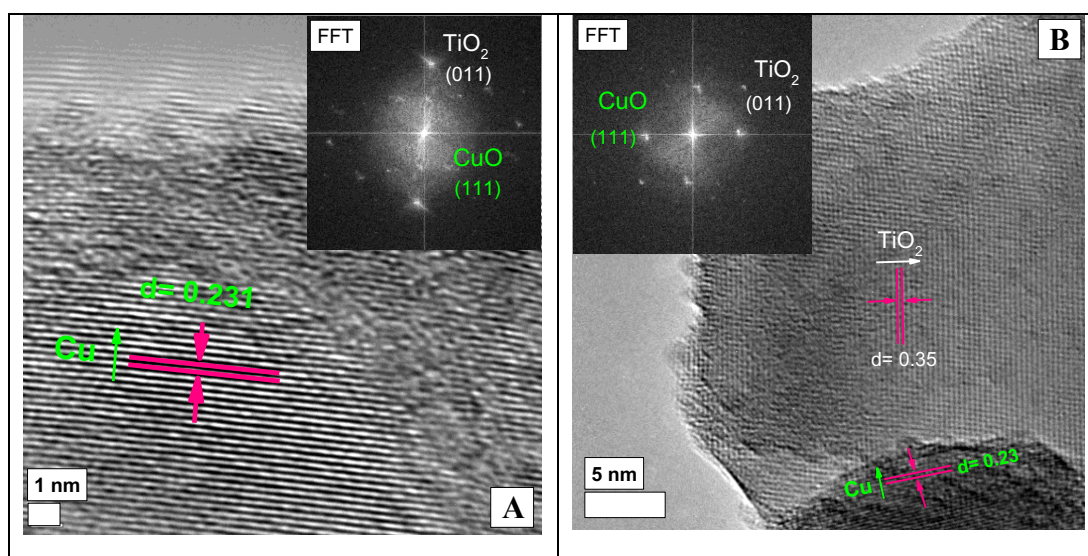


Figure 3. HR-TEM for fresh Cu(3%)/P25 sample calcined at 350 °C (**A**, inset: FFT analysis) and for fresh Cu(10%)/P25 catalyst calcined at 350 °C (**B**, inset: FFT analysis).

Changing Cu composition in Cu/P25 catalyst to 10% while maintaining the calcination temperature at 350 °C did not lead to a significant alteration in the catalyst structure (Figure 3B), however larger surface deposits were appreciated (Figure 3B). To further clarify the oxidation state of surface Cu-species, samples were analyzed by means of XPS analysis. Higher temperatures led to an increase of copper surface availability, as evident from Cu/Ti atomic ratio in Cu(3%)/P25 samples (Table S2). At 550 °C aggregation phenomena of copper particles can occur, resulting in higher Cu detected amount in the same analyzed spot. A similar trend is shown when the catalysts were prepared with increasing bulk copper loading, even at the lowest calcination temperature (Table S3). Actually, both the total copper increase and the eventual surface aggregation phenomena could contribute to the increase of copper amount detected on the surface. Indeed, the observed increase in Cu surface availability was not proportional to the overall Cu content; actual difference between them got wider with increasing copper loading, suggesting a different size distribution of copper species on TiO₂ surface. Apart from total surface copper availability, XPS measurements were aimed at elucidating Cu and Ti oxidation state of Ti on TiO₂ surface. Figure 4A shows Ti2p XP spectral region of fresh Cu(3%)/P25 and Cu(10%)/P25 catalysts. XPS spectra of all catalysts with different copper loadings are reported in Figure S5.

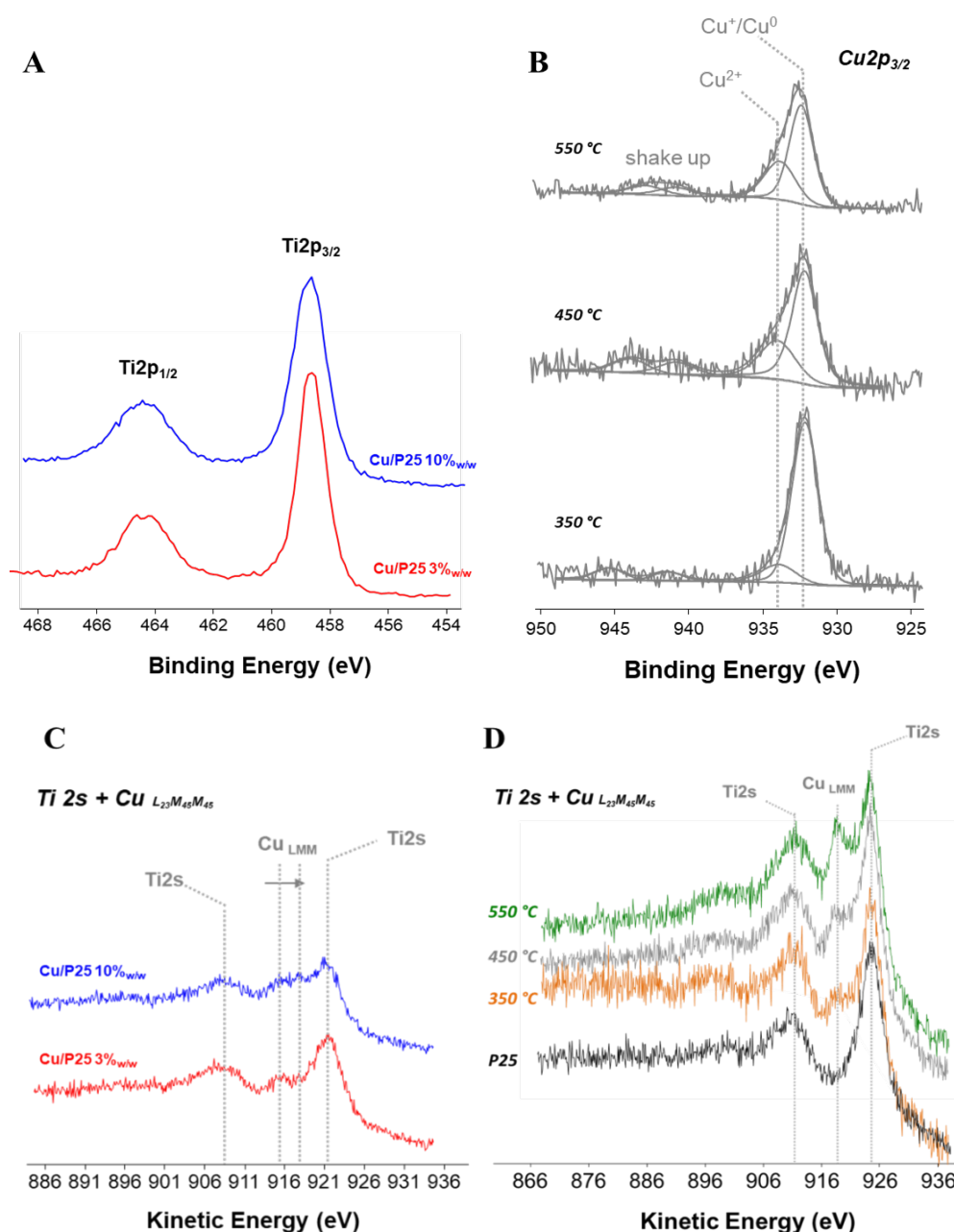


Figure 4. Ti2p XP spectra of the fresh Cu(3%)/P25 and Cu(10%)/P25 catalysts calcined at 350 °C (A). Cu2p_{3/2} XP spectra of the fresh Cu(3%)/P25 sample at different calcination temperatures (B). Ti2s XP+Cu_{LMM} XAE spectra of Cu(3%)/P25 and Cu(10%)/P25 calcined at 350 °C (C) and of Cu(3%)/P25 at different calcination temperatures (D).

In all the spectra, the characteristic peaks of Ti2p_{3/2} and Ti2p_{1/2} were observed at BE values of 458.7±0.1 eV and 464.4±0.1 eV, respectively, and were assigned to Ti⁴⁺ in TiO₂.^[1] A possible interaction between Cu species and P25 would result not only in the BE shift but also in the change of the spin-orbit splitting value in the Ti2p signal.^[1] Nevertheless, no significant variation was

observed neither changing the copper loading nor increasing the calcination temperature (Figure 4A, Figure S5 in Supplementary Information); the value was measured to be constant and equal to 5.7 eV, therefore no Cu incorporation into the TiO₂ lattice could be hypothesized.^[2] Figure 4B reports Cu2p_{3/2} XP spectra of the Cu(3%)/P25 catalyst calcined at different calcination temperatures. After curve-fitting procedures, the main peak was identified at BE=932.4±0.1 eV in all the cases and was ascribed to Cu⁺/Cu⁰ species.^[1,3] Furthermore, shake up satellites were visible (940-945 eV) along with a peak at 934.0±0.1 eV, that was assigned to Cu²⁺ species.^[1,3] The copper spectral regions of the catalysts prepared at higher bulk copper loadings (Figure 4A, Figure S5) as well as at different calcination temperatures (Figure 4B) showed similar results. Particularly, for Cu(3%)/P25 sample at different temperatures, a main peak due to Cu⁺/Cu⁰ species along with variable amounts of Cu²⁺, depending on the Cu loading, was detected (Figure 4B). Since the binding energies of Cu⁺ and Cu⁰ are not distinguishable based on Cu2p_{3/2} XP peak, the spectral region relative to X-ray excited Auger copper spectra (XAES Cu_{LMM}) were investigated to fully elucidate the oxidation state of the reduced copper species. Figure 4 reports Cu_{LMM} spectra for fresh Cu(3%)/P25 and Cu(10%)/P25 samples treated at 350 °C (C) and 3%Cu bulk loading at different calcination temperatures (D) .

A further challenge in the Cu⁺/Cu⁰ discrimination was represented from the partial overlapping of Cu_{LMM} and the predominant Ti2s spectral regions (black line in Figure 4D). Nevertheless, the main peak for copper was still detectable in all the samples and was found at KE=916.3±0.3 eV. Moreover, the Auger parameter – the sum of the binding energy from XPS and the kinetic energy from XAES – was calculated to be 1848.7±0.1 eV. Both the values demonstrated that the Cu⁺/Cu⁰ peak is ascribable to Cu⁺ species.^[3] However, the absence of Cu⁰ traces could not be completely ruled out under these experimental conditions, since the peak would fall at KE=918.6 ±0.2 eV, overlapped with Ti2s peak.^[46] Similar results were obtained for XPS spectra of the samples at different calcination temperatures (Figure 4D). When the relative abundance of Cu²⁺ is increased, the peak is shifted to slightly higher KE values, according to KE values for oxidized copper species (Figure 4C).^[3]

To get a greater insight into the Cu-TiO₂ interaction as function of the annealing temperature, the reducibility of the samples was studied by means of the TPR technique. The TPR profile of Cu(3%)/P25 sample after calcination at 350 °C is shown in Figure 5A, while the TPR profiles of Cu(3%)/P25 sample after calcination at 250, 450 and 550 °C are reported in Figure S6 (Supplementary Information). All of them are reported in the temperature range characteristic of copper oxide reduction,^[22,38,52] where instead TiO₂ reduction was hardly observed.

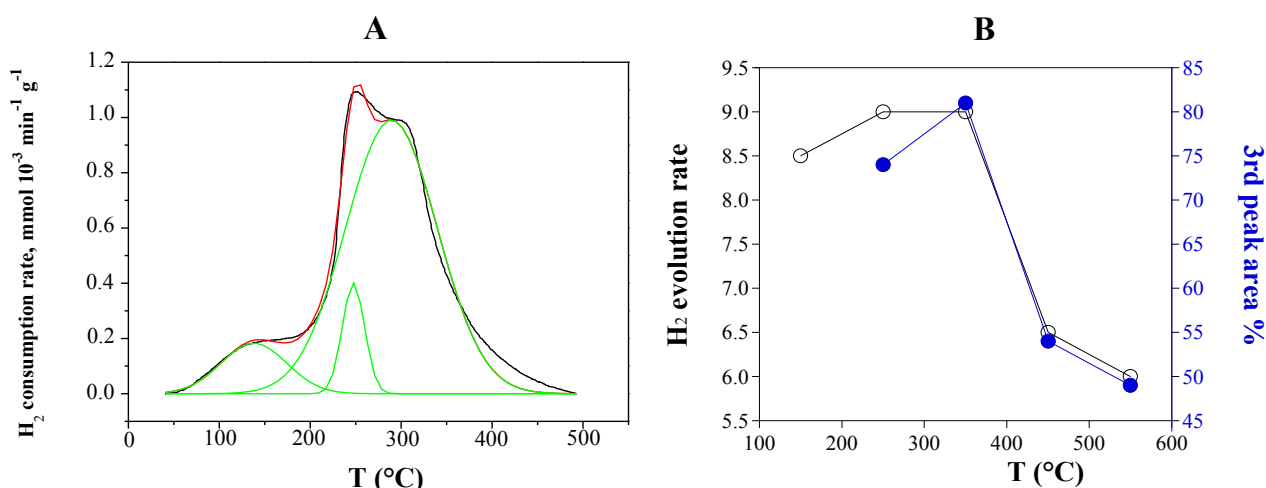


Figure 5. Panel A: TPR profile of Cu(3%)/P25 sample calcined at 350 °C. **Panel B:** H₂ evolution rate (○) and percentage of TPR 3rd peak area (●) as a function of calcination temperature for Cu(3%)/P25 sample.

As indicated by the curve fit analysis, the samples showed a distribution of copper species; conversely, the unsupported CuO showed a single peak at 400 °C.^[45,46] The hydrogen consumption relative to each fitting peak for Cu(3%)/P25 is listed in Table 2 and Table S4 along with T_{max} values.

Table 2 - Results of TPR measurements for fresh Cu(3%)/P25 sample calcined at 350 °C

Sample	T _{max} (°C)	Hydrogen consumption (μmol/g)
Cu(3%)/P25	138, 246, 290	101, 76, 759

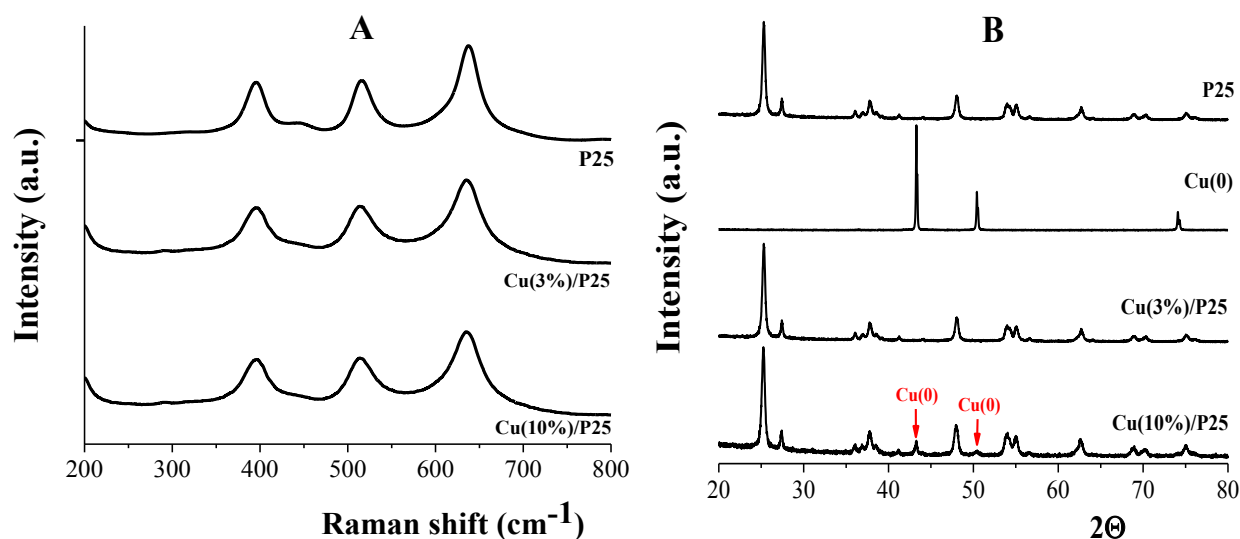
The assignment of the reduction peak at lower temperature is quite controversial: it is generally ascribed to the reduction of highly reducible Cu²⁺ species, though the presence of Cu⁺ species cannot

289 be ruled out.^[38] Indeed, Chen et al. ^[22] assigned the TPR peak in this range to the reduction of Cu⁺
290 species in Cu(3%)/P25 sample. The formation of Cu⁺ species was ascribed to the presence of oxygen-
291 defect vacancies in the TiO₂ structure. The presence of isolated Cu⁺ species and small Cu₂O cluster
292 with reduction peak at 157 °C and 208 °C, respectively was also proposed by Minsu Jung et al.^[52,53]
293 Samples treated at 250 °C and 350 °C, *i.e.* Cu(3%)/P25_250 and Cu(3%)/P25_350, showed the
294 highest hydrogen consumption in correspondence of the peak at about 280-290 °C associable to small
295 and/or highly dispersed CuO particles. TPR profile gradually changed by increasing the calcination
296 temperature, leading to a decrease of the peak at 280-290 °C and to the occurrence of another
297 reduction peak at higher temperature. Peaks located in the 320-400 °C temperature range are
298 indicative of the formation of bulky CuO species.^[45,46] Thus, it can be inferred that a lower calcination
299 temperature resulted in a better dispersion of copper species on the support. As far as the overall H₂
300 consumption is concerned, it was much higher with respect to the stoichiometric amount as calculated
301 under the hypothesis of the occurrence of all Cu as Cu²⁺ species. This likely indicated some spillover
302 phenomena of H₂ occurring over the support with the likely partial reduction of the latter, as generally
303 observed for copper doped anatase.^[54]
304 The influence of calcination temperature on hydrogen production rate is reported in Figure 5B,
305 together with the percentage of amount of the third peak area in TPR analysis. Actually, evolved H₂
306 amount appeared closely related to the fraction of highly dispersed CuO particles strongly interacting
307 with the support, probably accounting for the third peak area in TPR analysis (Table 2 and Table S4).

308 **Characterization of the used Cu/P25 photocatalysts**

309 The Cu/P25 catalysts were also analyzed after their use to assess any evolution of Cu oxidative state
310 during photocatalytic runs, so as to identify the nature of Cu-active species towards H₂ evolution as
311 well as their role in photocatalytic. Particularly, this investigation was carried out on both
312 Cu(3%)/P25 and Cu(10%)/P25 samples, calcined at 350 °C. Specifically, Raman spectra of both
313 samples after photocatalytic run, reported in Figure 6A, indicated that no peak ascribable to the

314 presence of cupric species was observed. This result was also confirmed by the EPR evidence
 315 indicating that these considered samples did not show any paramagnetic signal. Since no significant
 316 release of cupric ions was observed during photoreforming tests, obtained results suggest the
 317 reduction of the copper during the photoreforming process. Actually, the indigo color of the final
 318 suspension supported a change of the oxidation state of copper deposited on titania, further confirmed
 319 by XRD diffraction analysis too. Notably, XRD patterns of used Cu(10%)/P25 collected after the
 320 photocatalytic run, no longer showed diffraction peaks of CuO phase and clearly indicated the
 321 presence of Cu(0) diffraction peaks (Figure 6B). Unfortunately, due to the low Cu content, this peak
 322 was not detectable in the XRD spectrum of the used Cu(3%)/P25 sample.



323
 324 **Figure 6. Panel A:** Raman spectra of bare P25, used Cu(3%)/P25 and Cu(10%)/P25 samples calcined
 325 at 350 °C for 5h. **Panel B:** XRD patterns of bare P25, Cu(0), used Cu(3%)/P25 and Cu(10%)/P25
 326 calcined at 350 °C for 5h.

328 HR-TEM and FFT analyses were performed on used Cu(3%)/P25 catalyst calcined at 350 °C, showing
 329 co-existence of Cu₂O and Cu⁰ on the TiO₂ particles, thus indicating CuO reduction (Figures 7) during
 330 the photocatalytic experiment. It is noteworthy mentioning the co-existence of Cu₂O and Cu⁰ in the
 331 used Cu/P25 catalysts was deduced from the indicated phase (111) that corresponds to both Cu₂O and
 332 Cu⁰,^[55] the latter also confirmed by XRD analysis. Again, Cu₂O (111) and Cu⁰ (111) were the
 333 dominant copper species in the 10%Cu-containing catalyst (Figure S7).

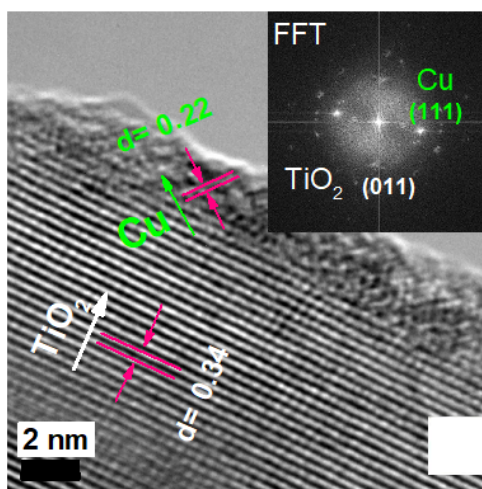


Figure 7. HR-TEM for used Cu(3%)/P25 sample calcined at 350 °C.

The comparison of XPS copper spectra of Cu(3%)/P25 before and after use are reported in Figure 8 while Cu/Ti ratio for the same samples are reported in Table S5 (Supplementary Information).

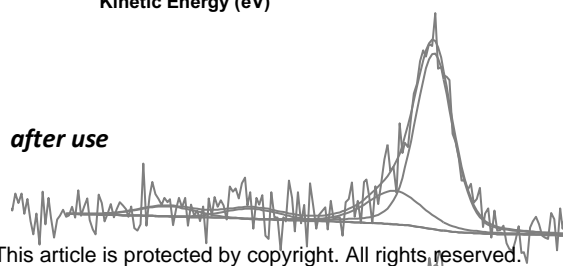
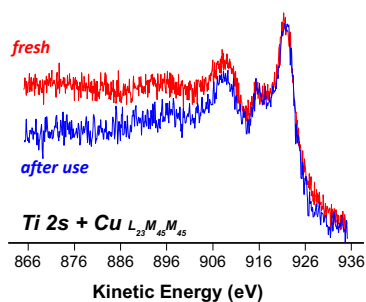
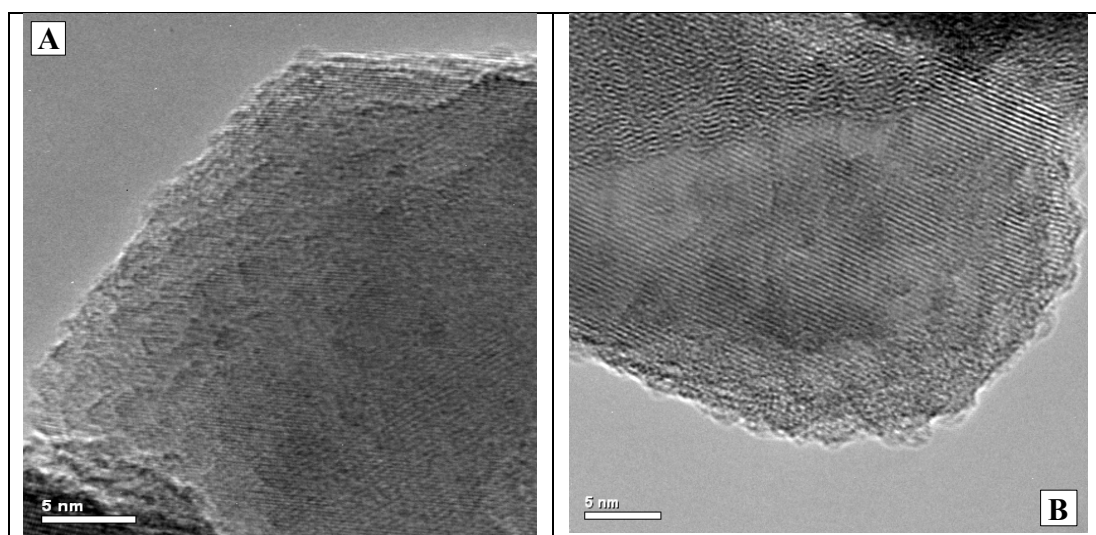


Figure 8. Cu2p_{3/2} XP spectra for Cu(3%)/P25_350°C fresh and after use. Corresponding Cu_{LMM} XAE spectra in the inset.

From XPS and XAES results no specific differences could be derived on the surface of the catalyst before and after use. Both spectra presented a small amount of Cu²⁺ (peak at BE=, 934.0±0.1 eV, along with shake up features) and the predominant Cu⁺/Cu⁰ oxidation state on the catalyst's surface (main peak at BE=932.4±0.1 eV). Moreover, XAES peaks are completely overlapped. Furthermore, Cu⁰ peak, if any, is overlapped with Ti2s peak in XAE spectrum: this makes any possible change in Cu⁰ amount hardly appreciable in the studied systems.^[49] Finally, Cu/Ti ratio slightly increased after use (Table S5), probably due a different distribution of surface copper species.

Despite Cu-doped TiO₂ catalysts have been intensively studied for H₂ production through photo-reforming, published results are still controversial on the activity of different Cu oxidation states.^{[20,26-}

34] Our results clearly showed that calcination of $\text{Cu}(\text{NO}_3)_2 \times 3\text{H}_2\text{O}$ -impregnated P25 samples under nitrogen atmosphere leads to a mixture of CuO and Cu_2O nanostructures on P25 surface. The former was clearly evidenced by bulk characterization techniques, in particular EPR and Raman spectroscopy. Furthermore, XPS analysis proved the presence of surface Cu_2O as the predominant CuO_x species. The poor CuO amount measured through this methodology, can be explained considering this technique revealing composition of the more exposed layer on the surface. These results supported earlier reports, where both oxidation states are observed for copper.^[22,24-28,36] Furthermore, as a major point, from TPR analysis different populations of CuO_x species could be distinguished on the catalysts. A highly dispersed fraction of small and dispersed CuO particles strongly interacting with the support was appreciated on the catalysts with the highest H_2 evolution rate. During photocatalytic process, CuO_x based deposits were reduced to $\text{Cu}_2\text{O}/\text{Cu}^0$ and concurrently a morphological evolution was also appreciated (Figure 9). Notably, deposits with less defined morphology were observed in Cu(3%)/P25 sample after use, while larger CuO_x surface deposits were observed in Cu(10%)/P25 sample. Previous reports provided evidence of Cu^{2+} reduction to Cu^+ ^[22,36] and to Cu^0 ^[41] under UVA irradiation.



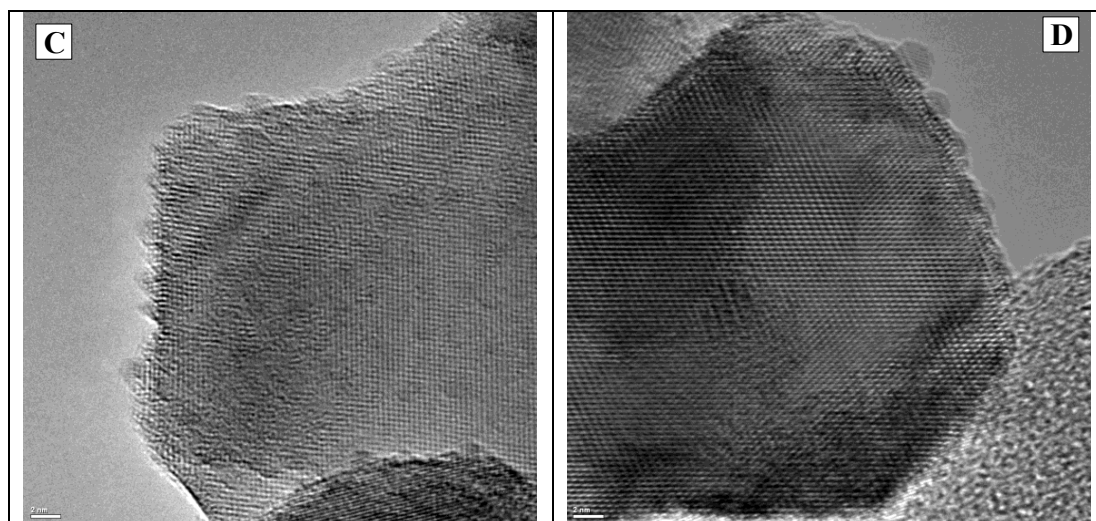
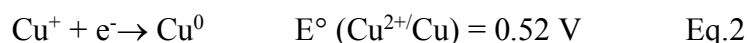
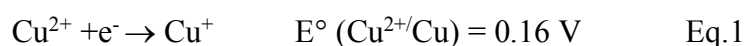
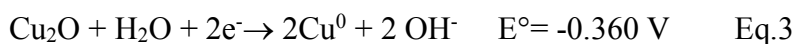


Figure 9. HR-TEM for Cu(3%)/P25 sample fresh (A) and after used (B) and for Cu(10%)/P25 sample, before (C) and after used (D).

Experimental findings and in particular morphological evolution from HR-TEM analysis as well as Cu changes in copper surface availability after use (Table S5, Supplementary Information) suggested that CuO_x species undergo in situ dynamic nanostructuring during photocatalytic run. The process is driven by the dissolution-redeposition of CuO_x deposits on the TiO_2 surface under UV irradiation.^[56-57] In more detail, CuO_x species must be involved in a dissolution process, leading to Cu^{2+} ions, that upon illumination are reduced to Cu_2O and then to Cu, by photo-generated electrons, according to Equations 1 and 2, both involving dissolved Cu ions:



In fact, electrochemical potentials of both half-reactions are higher than H^+ species, supporting the hypothesis of Cu^{2+} and Cu^+ preferential reduction by TiO_2 photogenerated electrons. The excess of electrons in the Cu deposits, accompanied by the consumption of photogenerated holes by methanol, allowed for the deposits to keep a metallic state throughout the reaction, as experimentally confirmed. Actually, negative electrochemical potential of solid state reduction further supports the hypothesis of reduction from solution (Equation 3).



Indeed, Cu_2O reduction to metallic Cu was not revealed by previous studies on Cu impregnated TiO_2 ,^[22] however these differences should depend on the size of CuO_x deposits and their interaction with TiO_2 surface, strongly influencing their reducibility.

Actually, change in size and distribution of Cu species on the surface, as evidenced by HR-TEM, supports this mechanism.

Actually, island-like morphology of copper species on TiO_2 surface suggests deposition-reduction process occurred according to the Volmer-Weber mechanism^[58]. Notably, the lattice parameters of the substrate, significantly affect the sizes and oxidation level of Copper deposits. On this basis, as evidenced by experimental results, Cu and Cu_2O species must be preferentially deposited on TiO_2 surface, due to their very good crystal lattice matching with P25 substrate ($a_{\text{Cu}} = 0,3615 \text{ nm}$, $a_{\text{TiO}_2 \text{ anatase}} = 0,378 \text{ nm}$; $a_{\text{Cu}_2\text{O}} = 0,427$, $a_{\text{TiO}_2 \text{ rutile}} = 0,459 \text{ nm}$). As a further support, electrochemical deposition on a semiconducting surface leads to coexistence of Cu and Cu_2O species on the surface.

Metallic Cu nanoparticles, should act as a co-catalyst for H_2 production, attracting photogenerated electrons from TiO_2 and promoting their transfer to the protons,^[27] according to the scheme in Figure 10.

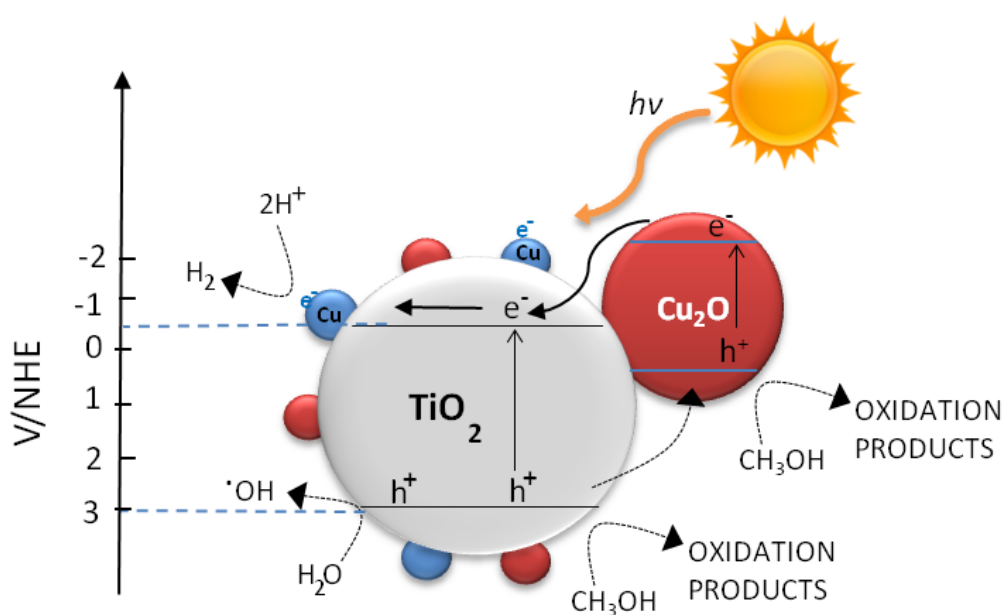


Figure 10. Proposed hydrogen photogeneration mechanism for Cu/Cu₂O/TiO₂ system.

433

434 At the same time, upon illumination, Cu_2O should inject photoelectrons into TiO_2 conduction band
435 and hosting holes from TiO_2 valence band (Figure 10). Electrons injected into TiO_2 bands should be
436 involved in H^+ reduction, thus accounting for H_2 production since the beginning of the photocatalytic
437 run. The increased presence of holes in Cu_2O may limit further reduction of the Cu^+ to Cu^0 as well as
438 methanol oxidation, thus accounting for constant pH values during photo-reforming. Both processes
439 restrict electron/hole recombination phenomena and account for improved photocatalytic activity of
440 Cu doped P25.^[27]

441

442 Conclusions

443 Altogether, our photocatalytic tests and the in-depth investigation on impregnated Cu/P25 systems
444 elucidated the nature of copper species active in hydrogen production on Cu/P25 systems. Our
445 findings showed that:

- 446 1) Both CuO and Cu_2O nanostructures were obtained onto Cu/P25 by impregnation and further heat
447 treatment in nitrogen.
- 448 2) The sample allowing the highest H_2 production rates showed the highest fraction of finely
449 dispersed CuO nanostructures, that during the photocatalytic process, CuO_x species undergo an
450 in situ dynamic nanostructuring, leading to a significant change in both oxidation state and size
451 distribution. This evolution is probably based on a dissolution-redeposition process. In particular,
452 CuO_x species were involved in a dissolution process, followed by reduction of Cu^{2+} ions to Cu^+
453 and Cu^0 by photo-generated electrons.
- 454 3) Both Cu_2O and Cu^0 acted as co-catalysts for H_2 generation. Upon illumination, the former injected
455 photoelectrons into TiO_2 conduction band. The latter acted as a co-catalyst, hosting
456 photogenerated electrons from TiO_2 and mediating their transfer to the protons. Both processes

restricted electron/hole recombination phenomena and accounted for improved photocatalytic activity of Cu doped P25.

The obtained findings clearly outline Cu/P25 catalysts as complex and dynamic systems. Their evolution during photocatalytic process must be influenced by solution properties as well as by preparation conditions of the catalyst itself, that markedly affect both size distribution and dispersion of Cu species, and ultimately lead to different ratios between copper oxidation states on the catalyst surface, thus affecting H_2 production rate.

The present work highlights that in situ catalysts transformation could improve their performance, laying the basis to explore this strategy to optimize activity of other catalytic systems.

Experimental Section

Materials

Methanol (99.8% v/v), P25-TiO₂ (80:20 anatase:rutile), sodium nitrite (NaNO₂, purity $\geq 97.0\%$) used as filter and cupric nitrite hydrate (Cu(NO₃)₂·3H₂O, purity 99.9%) were purchased from Sigma Aldrich. Bi-distilled water was used for the preparation of the reacting mixtures.

Cu/P25 material preparation

Copper (0.5, 3, 6, 10 and 16 wt %) was loaded on P25-TiO₂ by impregnation method.^[23] For each Cu-modified P25-TiO₂ sample (Cu/P25), a required amount of P25-TiO₂ was dispersed in Cu(NO₃)₂ aqueous solution. Excess water was evaporated to dryness with slow heating rate and constant stirring. The samples were dried at 110 °C and then calcined under nitrogen atmosphere for 5h at different temperatures ranging between 150 °C and 550 °C.

Photocatalytic runs

Photocatalytic runs were carried out in triplicate in an annular glass batch reactor (V=300 mL) covered with a layer of aluminum foil. The reactants and nitrogen gas were fed to the reactor through

its top inlet hole, while collection of outflow liquid and gaseous samples was performed at the bottom hole of the reactor at different reaction times. The reactor has been endowed with a high-pressure mercury vapor lamp (input power: 125 W) manufactured by Helios Italquartz emitting in both ultraviolet and visible range.

The lamp had ultraviolet emission peaks at 305, 313, and 366 nm corresponding to irradiances of 2.23×10^{-6} , 2.76×10^{-6} and 3.37×10^{-6} (E/s). The visible emission peaks at 405, 408, 436, and 546, corresponded to irradiances of 6.18×10^{-7} , 1.41×10^{-7} , 1.03×10^{-6} , and 1.16×10^{-6} E/s, respectively. The reactor was cooled at 25 °C during each run by means of a thermostatic bath (Falc GTR 90).

In order to evaluate the response of the photocatalytic system under visible light irradiation, during the experimental runs water in the cooling jacket was replaced by 1M NaNO₂ solution absorbing ultraviolet radiation, as reported elsewhere.^[40] The pH of the solution was monitored by means of an Orion 420A_p pH-meter (Thermo).

In order to avoid the undesired reaction of dissolved oxygen with photogenerated electrons, before starting the photocatalytic runs, a nitrogen stream was bubbled into the solution for 30 minutes for removing atmospheric oxygen. Moreover, throughout the experiments, nitrogen was continuously fed at a flow rate (Q_{N_2}) of 0.3 L/min to prevent any entrance of air into the reactor. For each run, fixed amounts of photocatalysts and methanol (10% v/v) were added to 300 mL of aqueous solution; the resulting suspension was sonicated and fed into the batch reactor under magnetic stirring. The liquid samples, collected at different reaction times, were quickly filtered on regenerated cellulose filters (pore diameter 0.20 μm, Scharlau) and the filtrate was used to measure dissolved copper and formic acid concentrations. The gaseous samples were recovered from the reactor outlet in Tedlar gas sampling bags and then used to evaluate hydrogen concentration.

Dissolved copper concentration was measured by means of a colorimetric method using an analytical kit (Macherey–Nagel) based on oxalic acid bis-cyclohexylidene hydrazide (cuprizone). A UV/Vis spectrometer (Cary 100 UV–Vis, Agilent) was employed for the measurements at a wavelength of 585 nm.

Hydrogen concentration was measured by a gas-chromatograph (Agilent 7820A) equipped with a HP-PLOT Molesieve 5A column (Agilent) and a TCD detector using argon as carrier gas. During the experiments, the radiation transmitted by the reactor was measured by means of a radiometer (not shown in the figure) in the range 315-400 nm and 401-1100 nm.

Physico-chemical characterization of the Cu/P25 nanomaterials

A physico-chemical investigation on Cu/P25 nanomaterials was performed by using a combined approach of different analytical techniques, such as High Resolution Transmission Electron Microscope (HR-TEM, X-Ray Diffraction (XRD), Temperature-Programmed Reduction (TPR), Raman, Electron Paramagnetic Resonance (EPR), and X-Ray Photoelectron Spectroscopy (XPS) spectroscopies. Also, the specific surface area (S_{BET}) of catalysts was also determined through BET porosimetry. Finally, H_2 Temperature Programmed Reduction (H_2 -TPR) analysis was also performed. The characterization was specifically focused on Cu(3%)/P25 and Cu(10%)/P25 catalysts before and after their use in the photo-reforming process.

BET analysis allowed determining the specific surface area (S_{BET}), that was evaluated by generating seven-point isotherms at 77 K for N_2 adsorption (Autosorb-1, Quantachrome) using the charred sample capable of providing a specific surface area equal to 5 m^2 in the sample cell.

Raman spectra of the prepared catalysts were performed by using a confocal Raman Microscope (Jasco, NRS-3100). Both the 514 nm line of an air-cooled Ar^+ laser (Melles Griot, 35 LAP 431-220) and the 647 nm line of a water-cooled Kr^+ laser (Coherent Innova 302C) were used. The laser line was injected into an integrated Olympus microscope and focused to a spot size of approximately 2 mm by using a $100\times$ or $20\times$ objective. A holographic notch filter was used to reject the excitation laser line. Raman scattering was collected by using a Peltier-cooled 1024×128 pixel CCD photon detector (Andor DU401BVI). For most systems, it took 60s to collect a complete data set. XRD measurements were performed using a PANalytical diffractometer with a nickel filter and Cu K_α radiation.

EPR experiments were carried out by means of X-band (9 GHz) Bruker Elexys E-500 spectrometer (Bruker, Rheinstetten, Germany), equipped with a super-high sensitivity probe head. Solid samples were transferred to flame-sealed glass capillaries which, in turn, were coaxially inserted in a standard 4 mm quartz sample tube. Measurements were performed at room temperature. The instrumental settings were as follows: sweep width, 1500 G; resolution, 1024 points; modulation frequency, 100 kHz; modulation amplitude, 1.0 G. 16 scans were accumulated to improve the signal-to-noise ratio. TPR measurements were carried out in a laboratory flow apparatus, using a 5% H₂/Ar ($Q=20\text{ cm}^3/\text{min}$), with a heating rate of 10 °C/min up to 800 °C. The sample (60 mg) was loaded in a quartz down-flow cell with a K thermocouple in close contact with the sample. The nanoparticles morphology and crystallinity were investigated using a JEOL (JEM-2010F) high resolution-transmittance electron microscope (HR-TEM) with the filed transmission of 200 kV. To prepare the samples for HR-TEM, the catalysts were suspended in ethyl alcohol and sonicated for 45 min, then fixed on a Lacy Carbon grid (LC300, EMS) by the drop-casting method. X-ray Photoelectron Spectroscopy (XPS) analysis was performed with a Versa Probe II Scanning XPS Microprobe spectrometer (Physical Electronics GmbH). The measurements were done with a monochromatized AlK α source (X-ray spot 100 μm), at a power of 24.4 W. Wide scans and detailed spectra were acquired in Fixed Analyzer Transmission (FAT) mode with a pass energy of 117.40 eV and 29.35 eV, respectively. An electron gun was used for charge compensation (1.0V 20.0 μA). All binding energies were referenced to C1s at 284.8 \pm 0.1 eV for adventitious hydrocarbon. Data processing were performed using MultiPak software v. 9.5.0.8.

553

554

555 References

- 556 [1] G. Colon, *Appl. Catal. A* **2016**, 518, 48-59.
557 [2] A.V. Puga, *Coord. Chem. Rev.* **2016**, 315, 1-66.
558 [3] J. M. Valero, S. Obregón, G. Colón, *Appl. Catal. B Environmental* **2015**, 179, 468-478.
559 [4] K. C. Christoforidis, P. Fornasiero, *ChemCatChem* **2017**, 9, 1523-1544.

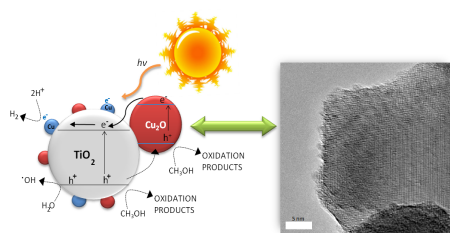
- [5] K. C. Christoforidis, P. Fornasiero, *ChemCatChem* **2019**, *11*, 368-382.
- [6] R. A. Rather, S. Singh, B. Pal, *J. Catal.* **2017**, *346*, 1-9.
- [7] T. Montini, M. Monai, A. Beltram, I. Romero-Ocaña, P. Fornasiero, *Mater. Sci. Semicond. Process* **2016**, *42*, 122-130.
- [8] M. Hinojosa-Reyes, R. Camposeco-Solís, R. Zanella, V. Rodríguez González, *Chemosphere*, **2017**, *184*, 992-1002.
- [9] M. R. Pai, A. M. Banerjee, S. A. Rawool, A. Singhal, C. Nayak, S. H. Ehrman, A. K. Tripathi, S. R. Bharadwaj, *Solar Energy Materials & Solar Cells* **2016**, *154*, 104-120.
- [10] M. Karnahl, E. Mejía, N. Rockstroh, S. Tschierlei, S. P. Luo, K. Grabow, A. Kruth, V. Brüser, H. Junge, S. Lochbrunner, M. Beller, *ChemCatChem* **2014**, *6*, 82-86.
- [11] D. Barreca, P. Fornasiero, A. Gasparotto, V. Gombac, C. Maccato, T. Montini, E. Tondello, *ChemSusChem* **2009**, *2*, 230-233.
- [12] T. Montini, V. Gombac, L. Sordelli, J.J. Delgado, X. Chen, G. Adami, P. Fornasiero, *ChemCatChem* **2011**, *3*, 574-577.
- [13] V. Gombac, L. Sordelli, T. Montini, J. J. Delgado, A. Adamski, G. Adami, M. Cargnello, S. Bernal, P. Fornasiero, *J. Phys. Chem. A* **2010**, *114*, 3916-3925.
- [14] F. Teng, M. Chen, N. Li, X. Hua, K. Wang, T. Xu, *ChemCatChem* **2014**, *6*, 842-847.
- [15] Z. Jiang, M. A. Isaacs, Z. W. Huang, W. Shangguan, Y. Deng, A. F. Lee, *ChemCatChem* **2017**, *9*, 4268-4274.
- [16] J. B. Priebe, J. Radnik, C. Kreyenschulte, A. J. J. Lennox, H. Junge, M. Beller, A. Brückner, *ChemCatChem* **2017**, *9*, 1025-1031.
- [17] D. Guerrero-Araque, P. Acevedo-Peña, D. Ramírez-Ortega, H. A. Calderon, R. Gomez, *Int. J. Hydrogen Energ.* **2017**, *42*, 9744-9753.
- [18] L. Clarizia, D. Spasiano, I. Di Somma, R. Marotta, R. Andreati, D.D. Dionysiou, *Int. J. Hydrogen Energ.* **2014**, *39*, 16812-16831.
- [19] A.J.J. Lennox, P. Bartels, M.M. Pohl, H. Junge, M. Beller, *J. Catal.* **2016**, *340*, 177-183.
- [20] Z. He, J. Fu, B. Cheng, J. Yu, S. Cao, *Appl. Catal. B* **2017**, *205*, 104-111.
- [21] L.S. Yoong, F.K. Chong, Binay K. Dutta, *Energy* **2009**, *34*, 1652-1661.
- [22] C. S. Chen, J. H. You, J. H. Lin, Y. Y. Chen, *Catalysis Communications* **2008**, *9*, 2381-2385.
- [23] C. S. Chen, T. C. Chen, C. C. Chen, Y. T. Lai, J. H. You, T. M. Chou, C. H. Chen, J. F. Lee, *Langmuir* **2012**, *28*, 9996-10006.
- [24] F. Boccuzzi, A. Chiorino, G. Martra, M. Gargano, N. Ravasio, B. Carrozzini, *J. Catal.* **1997**, *165*, 129-139.
- [25] F. Coloma, F. Marquez, C. H. Rochester, *Phys. Chem. Chem. Phys.* **2000**, *2*, 5320-5327.

- [26] G. Wu, N. Guan, L. Li, *Catal. Sci. Technol.* **2011**, *1*, 601–608.
- [27] K. Lalitha, G. Sadanandam, V. D. Kumari, M. Subrahmanyam, B. Sreedhar, N. Y. Hebalkar, *J. Phys. Chem. C* **2010**, *114*, 22181–22189.
- [28] M. Jung, J. N. Hart, J. Scott, Y. H. Ng, Y. Jiang, R. Amal, *Appl. Catal. A: General* **2016**, *521*, 190–201.
- [29] A. Heciak, A. W. Morawski, B. Grzmil, S. Mozia, *Appl. Catal. B: Environmental* **2013**, *140–141*, 108–114.
- [30] A. J. Simamora, T. L. Hsiung, F. C. Chang, T. C. Yang, C. Y. Liao, H. P. Wang, *Int. J. Hydrogen Energy* **2012**, *37*, 13855–13858.
- [31] J. Yu, Y. Hai, M. Jaroniec, *J. Coll. Interf. Sci.* **2011**, *357*, 223–228.
- [32] L. Li, L. Xu, W. Shi, J. Guan, *Int. J. Hydrogen Energy* **2013**, *38*, 816–822.
- [33] J. Bandara, C.P.K. Udawatta, C.S.K. Rajapakse, *Photochem. & Photobiol. Sci.* **2005**, *4*, 857–861.
- [34] S. Xu, D. D. Sun, *Int. J. Hydrogen Energy* **2009**, *34*, 6096–6104.
- [35] S. Xu, J. Ng, X. Zhang, H. Bai, D. D. Sun, *Int. J. Hydrogen Energy* **2010**, *35*, 5254–5261.
- [36] P. Khemthong, P. Photai, N. Grisdanurak, *Int. J. Hydrogen Energy* **2013**, *38*, 15992–16001.
- [37] A.L. Luna, M.A. Valenzuela, C. Colbeau-Justin, P. Vázquez, J.L. Rodriguez, J.R. Avendaño, S. Alfaro, S. Tirado, A. Garduño, J.M. De la Rosa, *Appl. Catal. A: General* **2016**, *521*, 140–148.
- [38] Z. Xi, C. Li, L. Zhang, M. Xing, J. Zhang, *Int. J. Hydrogen Energy* **2014**, *39*, 6345–6353.
- [39] J.M. Valero, S. Obregón, G. Colón, *ACS Catal.* **2014**, *4*, 3320–3329.
- [40] M. Jung, J. Scott, Y.H. Ng, Y. Jiang, R. Amal, *Int. J. Hydrogen Energy* **2014**, *39*, 12499–12506.
- [41] L. Clarizia, G. Vitiello, D. K. Pallotti, B. Silvestri, M. Nadagouda, S. Lettieri, G. Luciani, R. Andreozzi, P. Maddalena, R. Marotta, *Int. J. Hydrogen Energy* **2017**, *42*, 28349–28362.
- [42] D. M. Tobaldi, N. Rozman, M. Leoni, M. P. Seabra, A. S. Škapin, R. C. Pullar, J. A. Labrincha, *J. Phys. Chem. C* **2015**, *119*, 23658.
- [43] T.H. Fleisch, G. J. Mains, *Application of Surface Science* **1982**, *10*, 51–62.
- [44] P. Cheng, W. Li, T. Zhou, Y. Jin, M. Gu, *J. Photochem. Photobiology A Chem.* **2004**, *168*, 97–101.
- [45] A. Compaan, H. Z. Cummins, *Phys. Rev. B* **1972**, *6*, 4753.
- [46] H. F. Goldstein, Dai-sik Kim, Peter Y. Yu, L. C. Bourne, J-P. Chaminade, L. Nganga, *Phys. Rev. B* **1990**, *41*, 7192.
- [47] B. Choudhury, M. Dey, A. Choudhury, *Int. Nano Lett.* **2015**, *3*, 25.

- 627 [48] T. Oku, R. Motoyoshi, K. Fujimoto, T. Akiyama, B. Jeyadevan, J. Cuya, *J. Phys. Chem. Solids*
628 **2011**, 72, 1206-1211.
- 629 [49] N. Wongpisutpaisan, P. Charoonsuk, N. Vittayakorn, W. Pecharapa, *Energy Procedia* **2011**, 9,
630 404-409.
- 631 [50] J. F. Moulder, W. F. Stickle, P. E. Sobol and K. D. Bomben, *Handbook of X-Ray Photoelectron*
632 *Spectroscopy*, Physical Electronics Division, Perkin-Elmer Corp., Norwalk, **1995**.
- 633 [51] S. Esposito, M. Turco, G. Bagnasco, C. Cammarano, P. Pernice, A. Aronne, *Appl. Catal., A*
634 **2010**, 372, 48-57.
- 635 [52] S. Esposito, M. Turco, G. Bagnasco, C. Cammarano, P. Pernice, *Appl. Catal. A* **2011**, 403, 128-
636 135.
- 637 [53] M. Jung, H. Y. Ng, Y. Jiang, J. Scott, R. Amal, *Chemeca 2013: Challenging Tomorrow* **2013**,
638 214-217.
- 639 [54] G. Wu, N. Guan, L. Li, *Catal. Sci. & Technol.* **2011**, 1, 601-608.
- 640 [55] I. Rossetti, J. Lasso, E. Finocchio, G. Ramis, V. Nichele, M. Signoretto, A. Di Michele, *Appl.*
641 *Catal. A* **2014**, 477, 42-53.
- 642 [56] E. Aslan, I. H. Patir, M. Ersoz, *Chemistry-A European J.* **2015**, 21, 4585-4589.
- 643 [57] D.V. Shinde, Z. Dang, U. Petralanda, M. Palei, M. Wang, M. Prato, A. Cavalli, L. De Trizio
644 and L. Manna, *ACS Appl. Mater. Interfaces* **2018**, 10, 29583-29592.
- 645 [58] H. Bandarenka, S. L. Prischepa, R. Fittipaldi, A. Vecchione, P. Nenzi, M. Balucani and V.
646 Bondarenko, *Nanoscale Res. Lett.* , **2013**, 8, 85-93.

647

Accepted Manuscript

648 **Table of Contents**

649

650 CuO active species undergo in situ dynamic nanostructuring, through dissolution and photodeposition,
651 changing both oxidation state and size distribution

652